

Article

Dissolution and Solubility of the Calcite–Otavite Solid Solutions [(Ca_{1-x}Cd_x)CO₃] at 25 °C

Chengyou Ma¹, Fan Xu², Zongqiang Zhu^{3,*}, Hongqu Yang², Peijie Nong², Zhiqiang Kang¹, Shen Tang², Lihao Zhang² and Yinian Zhu^{4,*}

¹ College of Earth Sciences, Guilin University of Technology, Guilin 541006, China; machengyou2022@163.com (C.M.); zk99201@163.com (Z.K.)

² College of Environmental Science and Engineering, Guilin University of Technology, Guilin 541004, China; xufan6192022@163.com (F.X.); hongquyang@163.com (H.Y.); nongpeijie09@163.com (P.N.); tangshen@glut.edu.cn (S.T.); lhzhang@glut.edu.cn (L.Z.)

³ Guangxi Key Laboratory of Environmental Pollution Control Theory and Technology, Guilin University of Technology, Guilin 541004, China

⁴ Collaborative Innovation Center for Water Pollution Control and Water Safety in Karst Area, Guilin University of Technology, Guilin 541004, China

* Correspondence: zhuzongqiang@glut.edu.cn (Z.Z.); zhuyinian@glut.edu.cn (Y.Z.)

Abstract: A complete series of the calcite–otavite solid solutions [(Ca_{1-x}Cd_x)CO₃] were prepared, and their dissolution processes lasting nine months were experimentally investigated. For the dissolution in the N₂-degassed water, the Ca concentrations of the aqueous phases increased up to the steady states after 5040 h of dissolution, and the Cd concentrations of the aqueous phases increased up to the highest values and then decreased gradually to the steady states of 0.017–6.476 μmol/L after 5040 h of dissolution. For the dissolution in the CO₂-saturated water, the Ca and Cd concentrations of the aqueous phases increased up to the peak values and then decreased gradually to the steady states of 0.94–0.46 mmol/L and 0.046–9.643 μmol/L after 5040 h of dissolution, respectively. For the dissolution in the N₂-degassed water at 25 °C, the mean solubility products (log K_{sp}) and the Gibbs free energies of formation (ΔG_f^θ) were estimated to be –8.45–8.42 and –1129.65–1129.48 kJ/mol for calcite [CaCO₃] and –11.62–11.79 and –671.81–672.78 kJ/mol for otavite [CdCO₃], respectively. Generally, the log K_{sp} values decreased non-linearly, and the ΔG_f^θ values increased linearly with the increasing Cd/(Ca+Cd) mole ratio (X_{Cd}) of the (Ca_{1-x}Cd_x)CO₃ solid solutions. In the Lippmann diagrams constructed for the sub-regular (Ca_{1-x}Cd_x)CO₃ solid solutions with the estimated Guggenheim coefficients a₀ = –0.84 and a₁ = –3.80 for the dissolution in the N₂-degassed water or a₀ = –1.12 and a₁ = –3.83 for the dissolution in the CO₂-saturated water, the (Ca_{1-x}Cd_x)CO₃ solid solutions dissolved incongruently, moved progressively up to the quasi-equilibrium curves for otavite and then along the quasi-equilibrium curve from right to left, approached the *solutus* curve and finally reached the minimum stoichiometric saturation curve for calcite. The considerably Cd-poor aqueous phases were finally in equilibrium with the CdCO₃-rich solid phases.

Keywords: calcite; otavite; solid solution; dissolution; solubility; Lippmann diagram



Citation: Ma, C.; Xu, F.; Zhu, Z.; Yang, H.; Nong, P.; Kang, Z.; Tang, S.; Zhang, L.; Zhu, Y. Dissolution and Solubility of the Calcite–Otavite Solid Solutions [(Ca_{1-x}Cd_x)CO₃] at 25 °C. *Minerals* **2022**, *12*, 756. <https://doi.org/10.3390/min12060756>

Academic Editor: Felix Brandt

Received: 22 April 2022

Accepted: 12 June 2022

Published: 15 June 2022

Publisher's Note: MDPI stays neutral with regard to jurisdictional claims in published maps and institutional affiliations.



Copyright: © 2022 by the authors. Licensee MDPI, Basel, Switzerland. This article is an open access article distributed under the terms and conditions of the Creative Commons Attribution (CC BY) license (<https://creativecommons.org/licenses/by/4.0/>).

1. Introduction

Among toxic elements, the pollution of agricultural and natural environments by cadmium (Cd) is particularly a challenge, since it easily enters the alimental cycles, causing severe effects on the public health [1]. Out of water and soil, Cd can be absorbed by plants and enriched in animal bodies [2,3], leading to bone diseases and cancers [4,5].

Naturally, Cd presents only in minor amounts at the Earth's surface [2]. Its enrichment during weathering and soil formation of carbonate rocks, which normally contain a low Cd concentration, has caused large areas with the soil Cd concentration above the national guideline limit in many countries, including China [6–8]. Crystalline otavite [CdCO₃] has

been also found in minor amounts in rocks associated with nonferrous metal mines where natural Cd concentration is highest, and its precipitation may control Cd concentrations in polluted areas [2]. However, various anthropogenic activities, e.g., electrode manufacture, steel plating, metal smelting, printing and painting, have raised environmental Cd concentrations to an unsafe level in certain places [3,8].

Previous studies have demonstrated that the interaction of calcite with the Cd-bearing aqueous solution results in a reduction in the amount of Cd in water, which is principally of importance because calcite is almost ubiquitous in the environments and can have a strong effect on the behavior of many heavy metals, including cadmium, in shallow groundwater aquifers, marine sediments, and soils [2,3,9–13]. The study of the cadmium uptake by calcite suggested that the precipitation and coating of CdCO_3 on calcite predominated at higher Cd additions, whereas an ideal surface solid solution was formed between CdCO_3 and CaCO_3 for low Cd additions ($< 1 \mu\text{mol/g}$) [9]. This dramatic Cd-removing process has been interpreted as the rapid initial chemisorption of Cd at the calcite surface and the following formation of the calcite-otavite solid solution [5,10,14]. As a result, the aqueous Cd concentration can be decreased significantly to the values restricted by the low solubility of the Cd-rich endmembers [11,12,15].

Therefore, a deep understanding of the Cd^{2+} distribution between the aqueous and the solid phases is essential in order to reduce the cadmium concentrations in polluted waters from an environmental point of view [3]. Although there are some arguments about the ideal or non-ideal behavior of the calcite [CaCO_3] and otavite [CdCO_3] solid solution, most data show that Cd^{2+} (ionic radius 0.97 Å) has a nearly ideal character when substituting for Ca^{2+} (0.99 Å) in calcite [1,15–19].

Unfortunately, the skill to predict and simulate equilibrium condition in the solid solution–aqueous solution (SSAS) system is constrained, since thermodynamic dealing needs information about the properties of the solid solution and its two endmembers. The published data of the solubility products (K_{sp}) for otavite vary from $10^{-13.74}$ [20] to $10^{-9.98}$ [21], which is a difference of more than three orders of magnitude [2,11,22]. Calcite and otavite were suggested to form a nearly ideal solid solution with a Guggenheim parameter of $a_0 = -0.038 \pm 0.078$ [16], whereas a Guggenheim parameter of $a_0 = -0.8$ was estimated from the Cd-in-calcite distribution coefficients [23] and assuming a nearly ideal and regular solid solution of $\ln \gamma_{\text{CdCO}_3} = a_0[X_{\text{Cd}}]^2$ [24].

Briefly, information about the thermodynamic data of the calcite–otavite solid solution [$\text{Ca}_{1-x}\text{Cd}_x\text{CO}_3$] is still lacking due to a general lack of thermodynamic equilibrium in experiments lasting many days and the complex dissolution behavior of the solid solution, although its dissolution/precipitation can exert a considerable influence on the cadmium cycling in environments [10,11,25]. Thus, in the present work, with the aim of improving the thermodynamic data and models to describe and predict the SSAS interaction, the calcite–otavite solid solutions [$(\text{Ca}_{1-x}\text{Cd}_x)\text{CO}_3$] with the Cd/(Ca+Cd) mole ratio (X_{Cd}) of $0.00 \approx 1.00$ were prepared and analyzed by using different characterization techniques and then dissolved in aqueous solutions lasting nine months, in which the solution pH values and the release of different chemical species such as Cd^{2+} , Ca^{2+} and $\text{CO}_3^{2-}/\text{HCO}_3^-$ were monitored periodically. Lastly, the Lippmann diagrams for the $(\text{Ca}_{1-x}\text{Cd}_x)\text{CO}_3$ solid solutions were calculated and constructed to analyze the interaction and reaction paths in the SSAS system to assess the solubility of Cd-carbonates and the Cd distribution in aqueous environments.

2. Materials and Methods

2.1. Solid Synthesis

Well-crystallized solid samples (Cal-Ot-00–Cal-Ot-10) of the calcite–otavite solid solutions [$(\text{Ca}_{1-x}\text{Cd}_x)\text{CO}_3$] were prepared by mixing 2 mol/L Ca+Cd solution with 0.5 mol/L NH_3HCO_3 solution after the reaction of $\text{M}^{2+} + \text{CO}_3^{2-} = \text{MCO}_3$, where $\text{M} = (\text{Ca} + \text{Cd})$ (Table 1).

Table 1. Summary of synthesis and composition of the calcite–otavite solid solutions [(Ca_{1-x}Cd_x)CO₃].

Sample No.	Volume of Precursor (mL)			Amount of Precipitate (g)	Cd/(Ca+Cd) Mole Ratio			
	2 mol/L Ca(NO ₃) ₂	2 mol/L Cd(NO ₃) ₂	0.5 mol/L NH ₄ HCO ₃		Precursor Solution	Synthetic Solid	Solid after Dissolution in Water	
							N ₂ -Degassed	CO ₂ -Saturated
Cal-Ot-00	5.0	0.0	100	0.96	0.00	0.00	0.00	0.00
Cal-Ot-01	4.5	0.5	100	1.12	0.10	0.10	0.11	0.12
Cal-Ot-02	4.0	1.0	100	1.15	0.20	0.21	0.21	0.24
Cal-Ot-03	3.5	1.5	100	1.23	0.30	0.31	0.31	0.34
Cal-Ot-04	3.0	2.0	100	1.29	0.40	0.40	0.41	0.45
Cal-Ot-05	2.5	2.5	100	1.36	0.50	0.50	0.51	0.55
Cal-Ot-06	2.0	3.0	100	1.44	0.60	0.60	0.61	0.66
Cal-Ot-07	1.5	3.5	100	1.49	0.70	0.70	0.71	0.75
Cal-Ot-08	1.0	4.0	100	1.56	0.80	0.79	0.81	0.84
Cal-Ot-09	0.5	4.5	100	1.63	0.90	0.89	0.90	0.92
Cal-Ot-10	0.0	5.0	100	1.68	1.00	1.00	1.00	1.00

Pure water and chemicals of analytical reagent grade were employed to prepare the precursor solutions. The crystals were precipitated at room temperature (22 ± 1 °C) by dropping 5 mL of 2 mol/L mixture of Ca(NO₃)₂ and Cd(NO₃)₂ solutions at varied Cd/(Ca+Cd) mole ratios to 100 mL of the strongly stirred 0.5 mol/L NH₄HCO₃ solution under N₂ (Table 1). The suspended solutions were then stirred further for ten minutes. Lastly, the precipitates were cautiously separated from the suspensions using membrane filters, rinsed with CH₃CH₂OH and dried at 90 °C for 1 d.

2.2. Characterization

The bulk components of the solid samples obtained were determined by using the wet chemical analytic method. First, 10 mg of each sample was decomposed in 20 mL 1 mol/L HNO₃ solution and then diluted to 100 mL using pure water. The Ca and Cd concentrations were analyzed by an inductively coupled plasma-optical emission spectrometer (ICP-OES, Optima 7000DV, Perkin-Elmer Ltd., Waltham, MA, USA) with the detection limits of 0.01 mg/L or an atomic absorption spectrometer (AAS, PinAAcle 900T, Perkin-Elmer Ltd., Waltham, MA, USA) with the detection limits of 0.001 mg/L. All solid products were recognized crystallographically by comparing their X-ray diffraction spectra, which were obtained with an X-ray diffractometer (XRD, X'Pert PRO, PANalytical B.V., Almelo, The Netherlands) at the Cu K α radiation of 40 kV and 40 mA with a scan rate of 0.09°/min, with the references 01-083-0578 for calcite and 00-042-1342 for otavite of the International Center for Diffraction Data (ICDD). The solids were embedded in resins and coated using carbon to examine their morphological characters by a field-emission scanning electron microscope (FE-SEM, Jeol JEM-7800F, Tokyo, Japan).

2.3. Dissolution Experiment

Dissolution experiments in a closed system were performed. Instrumental-grade N₂ and CO₂ were used to saturate the initial solutions. The solution pH values were left to change freely without adjustments and recorded regularly. In the dissolution experiment with Cal-Ot-00–Cal-Ot-10, 10 g of the solid was weighed in a 5 L polyethylene terephthalate (PET) bottle, 5 L of the N₂-degassed water (initial pH 6.55) or the CO₂-saturated water (initial pH 3.89) was then filled into the bottle, which was capped and placed in an air-conditioned room at 25 °C. Then, 100 mL of the aqueous solution was regularly sampled from each bottle (1 h–270 d), and the temperature and pH value were recorded at the same time of sampling. Afterwards, 20 mL of the aqueous sample was filtered using 0.22 μ m membranes and instantly stabilized with 0.2% HNO₃ for the determination of Ca and Cd concentrations by ICP-OES. The total dissolved H₂CO₃⁰ concentrations (HCO₃+CO₃) were measured by an automatic potentiometric titrator (Metrohm 888 Titrand). After dissolution, the solid residues were sampled and examined using XRD and FE-SEM as well.

2.4. Thermodynamic Calculations

Firstly, the geochemical program PHREEQC (Version 3.7.3) [26] was applied to compute the free ion activities of Ca^{2+} , Cd^{2+} and CO_3^{2-} , and then, the ion activity product (IAP) was calculated after its definition, which equals the solubility product (K_{sp}) of the $(\text{Ca}_{1-x}\text{Cd}_x)\text{CO}_3$ solid solution at dissolution equilibrium. The species in the PHREEQC simulation included: Cd^{2+} , CdOH^+ , CdCO_3^0 , $\text{Cd}(\text{CO}_3)_2^{2-}$ and CdHCO_3^+ for cadmium; Ca^{2+} , CaOH^+ , CaHCO_3^+ and CaCO_3^0 for calcium; and CO_3^{2-} , HCO_3^- , H_2CO_3^0 , CaCO_3^0 , CaHCO_3^+ , CdCO_3^0 , $\text{Cd}(\text{CO}_3)_2^{2-}$ and CdHCO_3^+ for carbonate. The minteq.v4.dat database covered the thermodynamic properties for all aqueous species and solid phases involved in the simulation (Supplementary Material Table S1). The ionic strengths (<0.01433 mol/L) were within the valid limit for the extended Debye–Hückel equations.

3. Results and Discussion

3.1. Solid Characterization

3.1.1. Composition

The $\text{Cd}/(\text{Ca}+\text{Cd})$ mole ratio (X_{Cd}) of the synthetical calcite–otavite solid solution, which was calculated for the chemical compound with the formula of $(\text{Ca}_{1-x}\text{Cd}_x)\text{CO}_3$ when it was normalized to $\text{Ca}+\text{Cd} = 1.00$, was close to that of the precursor solution (Table 1). After their dissolution in the N_2 -degassed water and the CO_2 -saturated water for 270 d, the $\text{Cd}/(\text{Ca}+\text{Cd})$ mole ratios (X_{Cd}) of the solid residues increased slightly, particularly in dissolution in the CO_2 -saturated water.

3.1.2. XRD

All XRD patterns of the synthetical crystals were confirmed to be the $R\bar{3}c$ space group and belonged to the calcite–otavite solid solutions $[(\text{Ca}_{1-x}\text{Cd}_x)\text{CO}_3]$ (Figure 1). The most intense peaks (Position ($^\circ 2\theta$)/Intensity (%)/FWHM ($^\circ 2\theta$)/ hkl) for the synthetic solid of $X_{\text{Cd}} = 0.00$ (Cal–Ot–00) were 23.06/9.18/0.10/012, 29.41/100.00/0.13/104, 35.96/10.92/0.13/110, 39.41/18.35/0.10/113, 43.16/13.54/0.10/202, 47.51/14.56/0.10/018, 48.51/15.62/0.08/116 and 57.40/5.91/0.12/122, agreeing well with calcite (ICSD Reference code 01-083-0578). The most intense peaks (Position ($^\circ 2\theta$)/Intensity (%)/FWHM ($^\circ 2\theta$)/ hkl) for the synthetic solid of $X_{\text{Cd}} = 1.00$ (Cal–Ot–10) were 23.53/72.72/0.26/012, 30.34/100.00/0.20/104, 36.38/27.03/0.18/110, 40.09/3.56/0.51/113, 43.84/19.12/0.36/202, 48.15/11.11/0.41/018, 49.81/32.79/0.31/116 and 58.19/11.47/0.51/122, agreeing well with otavite (00-042-1342).

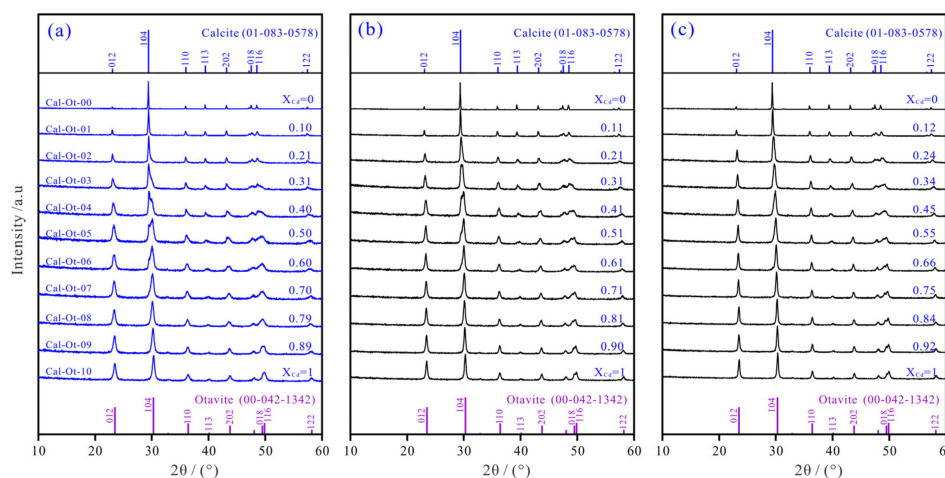


Figure 1. Diffraction patterns of the $(\text{Ca}_{1-x}\text{Cd}_x)\text{CO}_3$ solid solutions: (a) before dissolution and (b) after dissolution in the N_2 -degassed water for 270 d and (c) after dissolution in the CO_2 -saturated water for 270 d.

The reflection peaks, especially (104), moved a little to the higher angles with the increasing X_{Cd} of the solid solutions (Figure 1; Supplementary Material Figure S1), which

was due to the smaller interplanar distances of Cd-calcite than pure calcite. All solid phases varied only in their peak location, intensity, and width in the XRD patterns, suggesting that they were not a simple crystal mixture of calcite $[\text{CaCO}_3]$ and otavite $[\text{CdCO}_3]$, but rather the calcite–otavite solid solutions $[(\text{Ca}_{1-x}\text{Cd}_x)\text{CO}_3]$. After dissolution in the N_2 -degassed water and the CO_2 -saturated water for 270 d, no detectable changes were observed for all solid samples (Figure 1; Supplementary Material Figure S1).

3.1.3. SEM

The crystal morphologies of the synthetical calcite–otavite solid solutions $[(\text{Ca}_{1-x}\text{Cd}_x)\text{CO}_3]$ showed a strong reliance on the $\text{Cd}/(\text{Ca}+\text{Cd})$ mole ratios of the precursor solutions, showing the influence of Cd^{2+} (even at low concentrations) on the $\{104\}$ face growth of the calcite-type crystals [27–30]. The synthetical pure calcite (Cal-Ot-00) showed a rhombohedral morphology defined by the $\{104\}$ faces with the particle sizes of $\approx 10 \mu\text{m}$ (Figure 2). The sizes of the $(\text{Ca}_{1-x}\text{Cd}_x)\text{CO}_3$ solid solutions decreased with the increasing X_{Cd} , although their morphologies remained rhombohedral for the $(\text{Ca}_{1-x}\text{Cd}_x)\text{CO}_3$ aggregates (Figure 2; Supplementary Material Figure S2), which indicated that cadmium can affect the growth and morphology of the calcite-type crystals. As the X_{Cd} increased, the size of the individual crystal declined, and the $(\text{Ca}_{1-x}\text{Cd}_x)\text{CO}_3$ solid solutions and the endmember CdCO_3 ($X_{\text{Cd}}=0.10\text{--}1.00$; Cal-Ot-01–Cal-Ot-10) changed from coarse crystals to spherical aggregates of very fine small crystals (Figure 2). The spherical surfaces were characterized by the aggregation of plentiful minuscule blocks of $\{104\}$ faces that seemed somewhat disoriented, since they traced an external spherical shape. In addition, the decrease in the ‘physical’ spherical diameter with the increasing X_{Cd} was also observed.

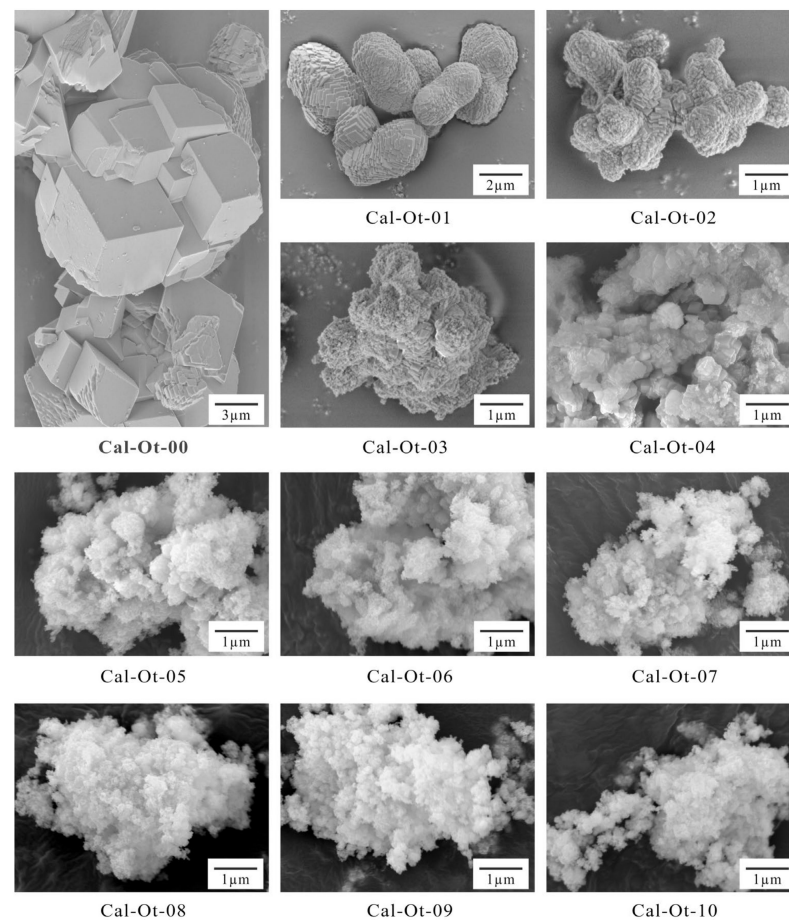


Figure 2. SEM images of the $(\text{Ca}_{1-x}\text{Cd}_x)\text{CO}_3$ solid solutions before dissolution.

Generally, all solids of the $(\text{Ca}_{1-x}\text{Cd}_x)\text{CO}_3$ solid solutions after dissolution in the N_2 -degassed water (Figure 3) and the CO_2 -saturated water (Figure 4) presented the same morphologic character as before; i.e., the solids changed from coarse crystals to spherical aggregates of very fine small crystals with the X_{Cd} increase. After dissolution, the edges of the calcite crystals degenerated, and etch pits on the surface could be found occasionally (Supplementary Material Figure S3).

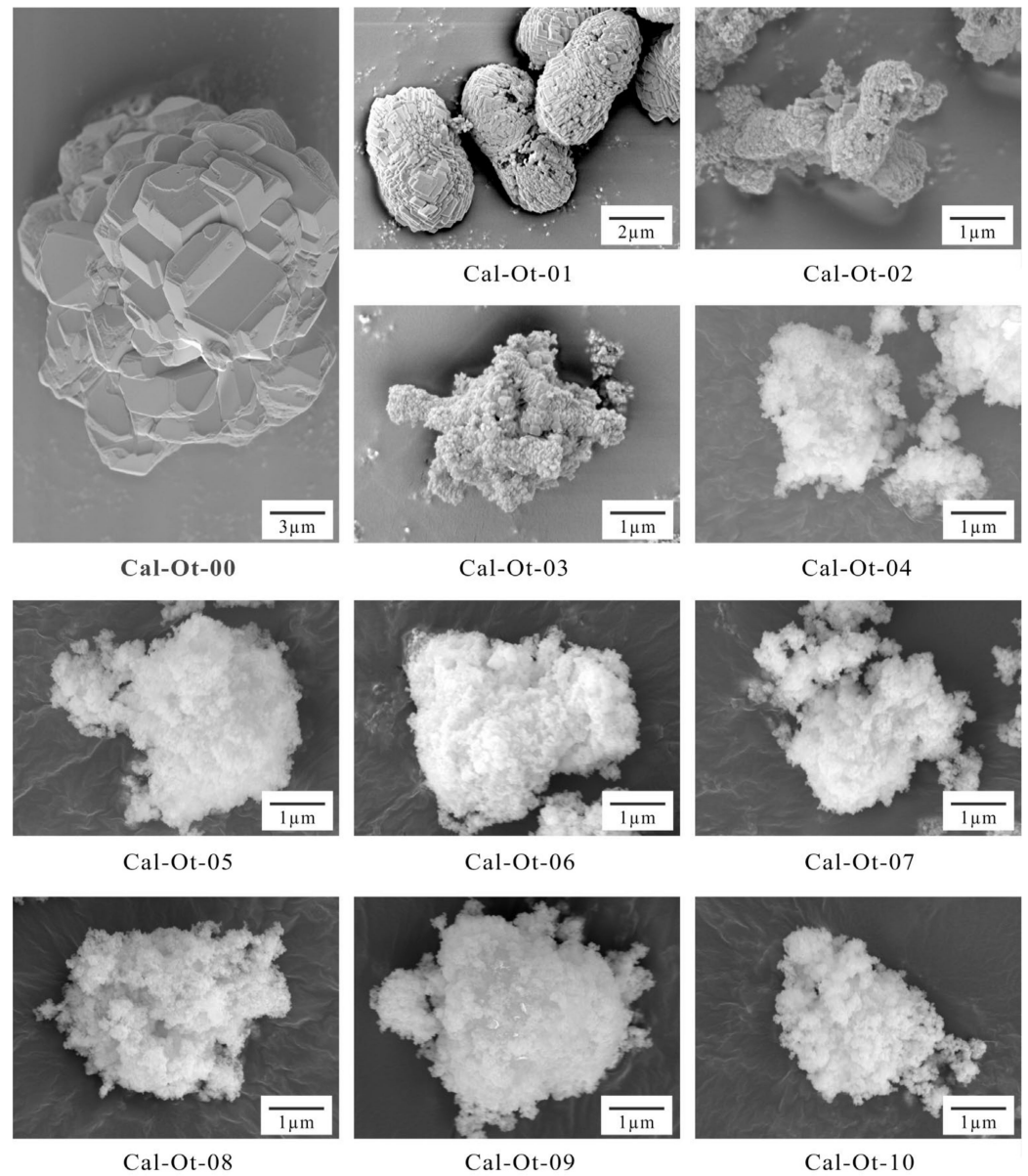


Figure 3. SEM images of the $(\text{Ca}_{1-x}\text{Cd}_x)\text{CO}_3$ solid solutions after dissolution in the N_2 -degassed water for 270 d.

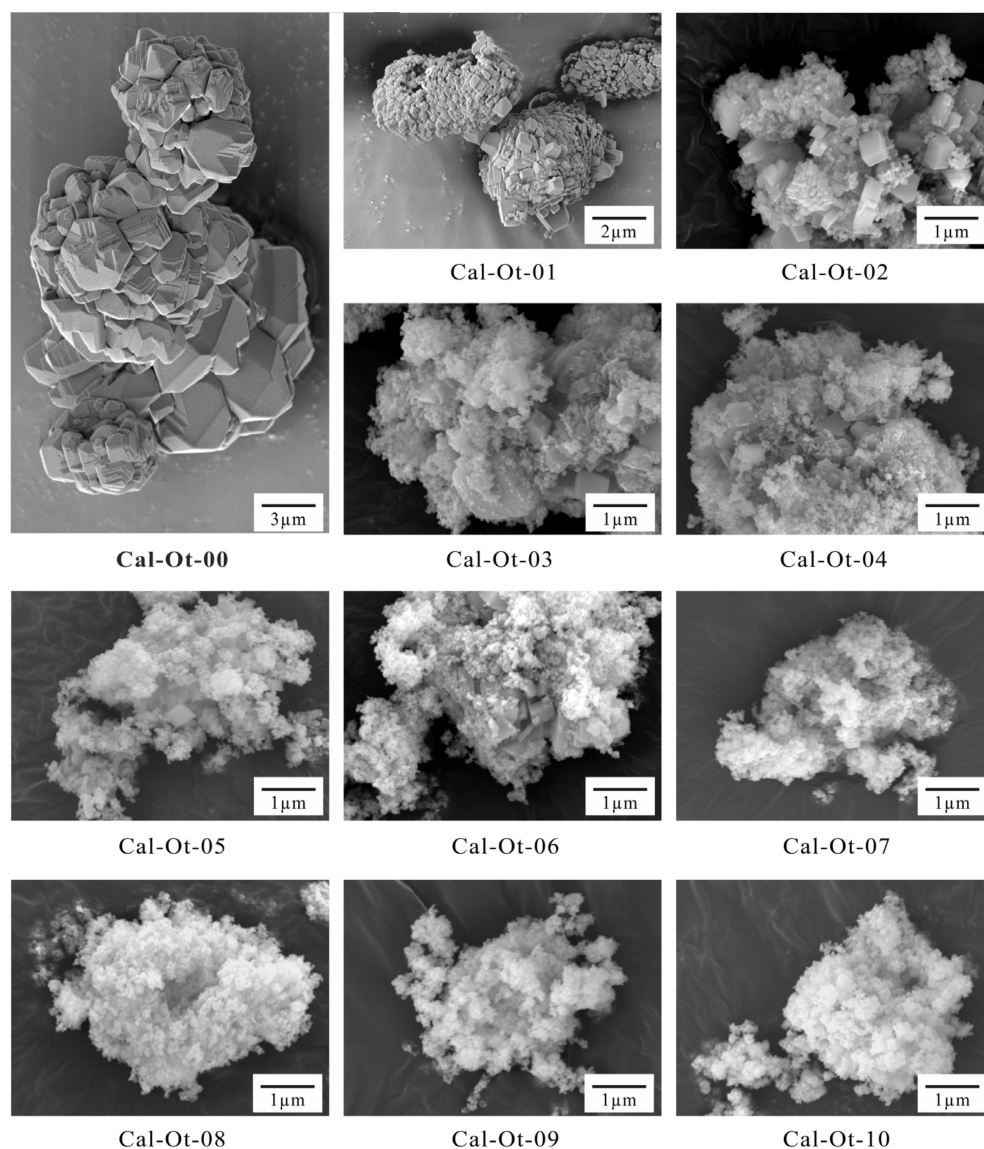


Figure 4. SEM images of the $(\text{Ca}_{1-x}\text{Cd}_x)\text{CO}_3$ solid solutions after dissolution in the CO_2 -saturated water for 270 d.

3.2. Change of the Aqueous Phase

For the dissolution in the N_2 -degassed pure water, the pH values of the aqueous phases increased from 6.55 up to the highest values of 9.81–8.45 in <1–1200 h and then decreased gradually to the steady states of 8.54–7.83 (Figure 5). The Ca and $\text{HCO}_3 + \text{CO}_3$ concentrations of the aqueous phases increased up to the steady states after 5040 h of dissolution for all solids of the $(\text{Ca,Cd})\text{CO}_3$ solid solutions. The Cd concentrations of the aqueous phases increased up to the highest values of 0.049–7.588 $\mu\text{mol/L}$ in <1–72 h and then decreased gradually to the steady states of 0.017–6.476 $\mu\text{mol/L}$ after 5040 h of dissolution (Figure 5). The Cd/(Ca+Cd) mole ratios were significantly smaller than the Cd/(Ca+Cd) mole ratios of the corresponding solids and decreased with time to a steady state (Supplementary Material Figure S4). Generally, the Cd concentrations of the aqueous phases at the last steady state increased, while the Ca and $\text{HCO}_3 + \text{CO}_3$ concentrations of the aqueous phases decreased with the increasing Cd/(Ca+Cd) mole ratios of the solids (Supplementary Material Figure S5).

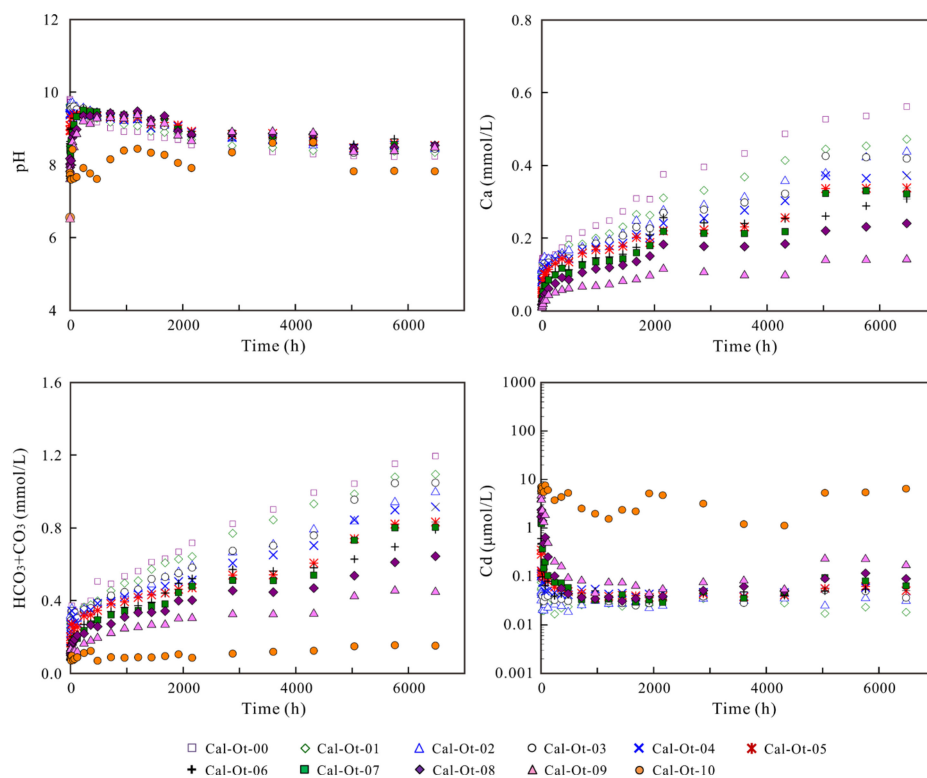
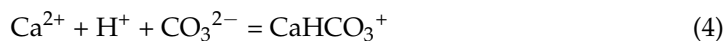


Figure 5. Change of the aqueous pH, the total dissolved calcium, the total dissolved cadmium and the total dissolved H_2CO_3^0 during the dissolution of the $(\text{Ca}_{1-x}\text{Cd}_x)\text{CO}_3$ solid solutions in the N_2 -degassed water.

For the dissolution in the CO_2 -saturated water, the pHs of the aqueous phases increased rapidly from 3.89 up to 5.67–4.92 in <1 h and then gradually to the steady states of 8.05–7.65 after 5040 h (Figure 6). The Ca and HCO_3+CO_3 concentrations of the aqueous phases increased up to the highest value of 6.14–0.58 mmol/L and 11.223–0.662 mmol/L after 48–1440 h and then decreased gradually to the last steady states of 0.94–0.46 mmol/L and 2.202~0.196 mmol/L, respectively (Figure 6). The Cd concentrations of the aqueous phases increased quickly up to the highest values of 68.943–470.239 $\mu\text{mol/L}$ in <1 h and then decreased gradually to the steady states of 0.046–9.643 $\mu\text{mol/L}$ after 5040 h of dissolution (Figure 6). The $\text{Cd}/(\text{Ca}+\text{Cd})$ mole ratios of the aqueous phases were obviously smaller than the $\text{Cd}/(\text{Ca}+\text{Cd})$ mole ratios of the corresponding solids and decreased with time to the steady states, indicating a non-stoichiometric release of Ca and Cd (Supplementary Material Figure S4).

Generally, the Cd concentrations of the aqueous phases at the steady state of dissolution increased with the increasing $\text{Cd}/(\text{Ca}+\text{Cd})$ mole ratios of the solids (Supplementary Material Figure S5). The Ca and HCO_3+CO_3 concentrations of the aqueous phases showed the highest values at $X_{\text{Cd}}=0.31\text{--}0.40$ (Cal-Ot-03–Cal-Ot-04) and then decreased as the X_{Cd} values decreased or increased (Supplementary Material Figure S5).

The dissolution of the $(\text{Ca}_{1-x}\text{Cd}_x)\text{CO}_3$ solid solutions is given as:



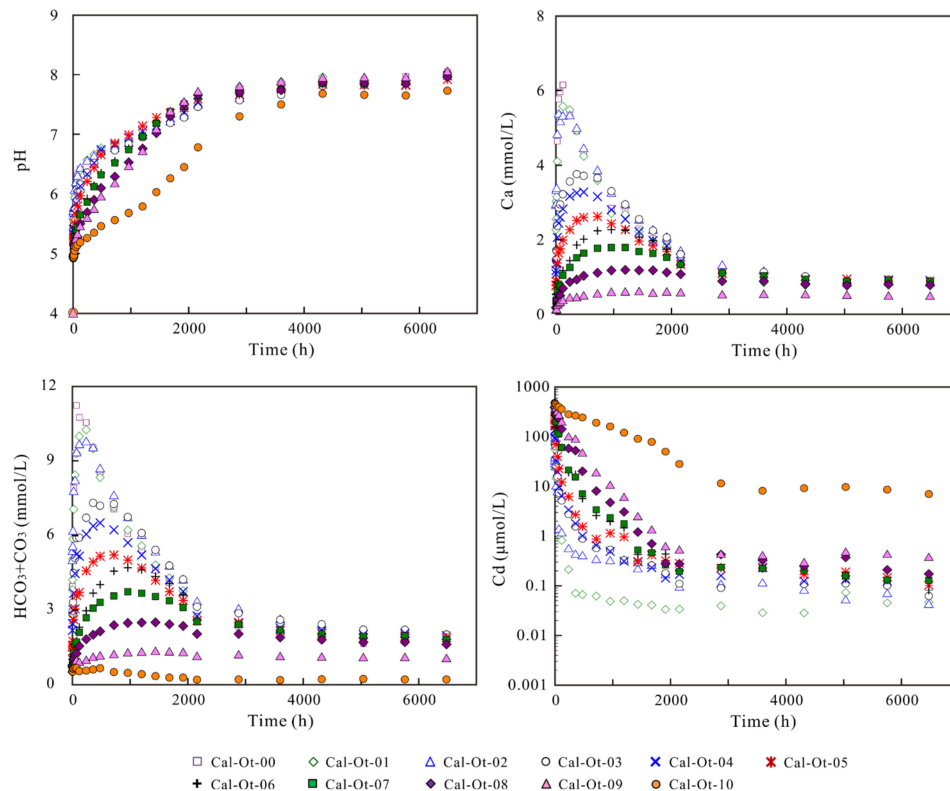
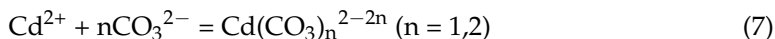
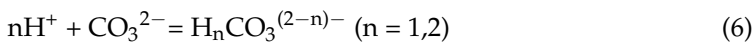


Figure 6. Change of the aqueous pH, the total dissolved calcium, the total dissolved cadmium and the total dissolved $H_2CO_3^0$ during the dissolution of the $(Ca_{1-x}Cd_x)CO_3$ solid solutions in the CO_2 -saturated water.

At the beginning of dissolution, all components were dissolved stoichiometrically (Equation (1)). For the dissolution in the N_2 -degassed water and the CO_2 -saturated water, the pH of the aqueous phase increases were ascribed to the formation of $CaHCO_3^+$, $CdHCO_3^+$ and $H_nCO_3^{(2-n)-}$ (Equations (4)–(6)), which resulted in the H^+ depletion. The notable pH variation showed that the initial dissolution was pH controlled [31,32]. More calcium was dissolved than cadmium, indicating that the $(Ca_{1-x}Cd_x)CO_3$ solid solutions dissolved non-stoichiometrically, which suggested the existence of an interface dissolution–precipitation process, and cadmium was more favorable for nucleation on the crystal surfaces to form new precipitates with a higher X_{Cd} .

3.3. Determination of the Stoichiometric Solubility

The dissolution experiments were performed until the difference in the IAP values with respect to each solid computed from the last three solution samples (i.e., 5040 h, 5760 h and 6480 h, supposing the steady states were attained) were <0.25 log units. The results of the PHREEQC simulations revealed that all aqueous phases in this work were unsaturated with respect to any likely secondary minerals, such as $Ca(OH)_2$ [portlandite] and $Cd(OH)_2$.

The thermodynamic solubility product (K_{sp}) can be estimated from the longstanding steady state or extrapolated from the ion activity product (IAP) that corresponds to the equilibrium constant of the mineral dissolution [33]. The K_{sp} values for the $(Ca_{1-x}Cd_x)CO_3$ solid solutions after the dissolution reaction Equation (1) at equilibrium can be calculated according to Equation (8):

$$K_{sp} = IAP = \{Ca^{2+}\}^{1-x}\{Cd^{2+}\}^x\{CO_3^{2-}\} \tag{8}$$

where {} designates the free ion activity.

The standard free energy of reaction (ΔG_r^θ) can be obtained from K_{sp} at 298.15 K and 0.101 MPa according to Equation (9):

$$\Delta G_r^\theta = -5.708 \log K_{sp} \tag{9}$$

For Equation (1),

$$\Delta G_r^\theta = (1-x)\Delta G_f^\theta[Ca^{2+}] + x\Delta G_f^\theta[Cd^{2+}] + \Delta G_f^\theta[CO_3^{2-}] - \Delta G_f^\theta[(Ca_{1-x}Cd_x)CO_3] \tag{10}$$

Rearranging,

$$\Delta G_f^\theta[(Ca_{1-x}Cd_x)CO_3] = (1-x)\Delta G_f^\theta[Ca^{2+}] + x\Delta G_f^\theta[Cd^{2+}] + \Delta G_f^\theta[CO_3^{2-}] - \Delta G_r^\theta \tag{11}$$

Tables 2 and 3 list the analytical results of the solution pH, Ca, Cd and HCO_3^-/CO_3^{2-} concentrations as well as the calculated log IAP values at the last steady state ($\approx \log K_{sp}$) for the dissolution of the $(Ca_{1-x}Cd_x)CO_3$ solid solutions. By using the thermodynamic data, $\Delta G_f^\theta[Ca^{2+}] = -553.54$ kJ/mol, $\Delta G_f^\theta[Cd^{2+}] = -77.58$ kJ/mol and $\Delta G_f^\theta[CO_3^{2-}] = -527.9$ kJ/mol [34], the Gibbs free energies of formation for the $(Ca_{1-x}Cd_x)CO_3$ solid solutions, $\Delta G_f^\theta[(Ca_{1-x}Cd_x)CO_3]$, were also estimated.

Table 2. Analytical data and solubility for the calcite–otavite solid solutions $[(Ca_{1-x}Cd_x)CO_3]$ in the N_2 -degassed water at 25 °C.

Sample	Dissolution Time (h)	pH	Concentration			# log IAP	Mean log IAP	ΔG_f^θ (kJ/mol)	Mean ΔG_f^θ (kJ/mol)
			Ca (mmol/L)	Cd (μ mol/L)	$HCO_3^-+CO_3^{2-}$ (mmol/L)				
^a $(Ca_{1.00}Cd_{0.00})CO_3$	5040	8.25	0.527		1.043	−8.48	−8.45	−1129.84	−1129.65
	5760	8.23	0.536		1.153	−8.45	±0.04	−1129.68	±0.22
	6480	8.24	0.562		1.195	−8.41		−1129.43	
^b $(Ca_{1.00}Cd_{0.00})CO_3$	5040	8.29	0.511		1.035	−8.45	−8.42	−1129.70	−1129.48
	5760	8.27	0.512		1.145	−8.43	±0.06	−1129.57	±0.30
	6480	8.32	0.534		1.154	−8.36		−1129.18	
* $(Ca_{0.90}Cd_{0.10})CO_3$ ** $(Ca_{0.89}Cd_{0.11})CO_3$	5040	8.37	0.445	0.017	0.987	−8.95	−8.91	−1080.14	−1079.93
	5760	8.38	0.454	0.023	1.080	−8.88	±0.04	−1079.76	±0.21
	6480	8.35	0.472	0.018	1.095	−8.90		−1079.88	
* $(Ca_{0.79}Cd_{0.21})CO_3$ ** $(Ca_{0.79}Cd_{0.21})CO_3$	5040	8.50	0.378	0.025	0.836	−9.35	−9.29	−1034.88	−1034.50
	5760	8.51	0.422	0.035	0.942	−9.23	±0.06	−1034.19	±0.38
	6480	8.44	0.438	0.031	0.996	−9.27		−1034.43	
* $(Ca_{0.69}Cd_{0.31})CO_3$ ** $(Ca_{0.69}Cd_{0.31})CO_3$	5040	8.34	0.426	0.052	0.955	−9.75	−9.68	−989.52	−989.13
	5760	8.44	0.423	0.049	1.046	−9.63	±0.07	−988.85	±0.39
	6480	8.45	0.419	0.036	1.049	−9.66		−989.04	
* $(Ca_{0.60}Cd_{0.40})CO_3$ ** $(Ca_{0.59}Cd_{0.41})CO_3$	5040	8.45	0.372	0.056	0.844	−10.11	−10.05	−943.99	−943.65
	5760	8.55	0.365	0.058	0.899	−9.99	±0.06	−943.34	±0.34
	6480	8.51	0.372	0.050	0.916	−10.04		−943.62	
* $(Ca_{0.50}Cd_{0.50})CO_3$ ** $(Ca_{0.49}Cd_{0.51})CO_3$	5040	8.48	0.337	0.057	0.741	−10.54	−10.46	−898.84	−898.39
	5760	8.60	0.338	0.062	0.821	−10.37	±0.09	−897.91	±0.48
	6480	8.54	0.339	0.051	0.833	−10.46		−898.42	
* $(Ca_{0.40}Cd_{0.60})CO_3$ ** $(Ca_{0.39}Cd_{0.61})CO_3$	5040	8.57	0.261	0.050	0.629	−10.98	−10.86	−853.75	−853.09
	5760	8.72	0.289	0.054	0.696	−10.78	±0.12	−852.62	±0.66
	6480	8.51	0.308	0.071	0.791	−10.82		−852.89	
* $(Ca_{0.30}Cd_{0.70})CO_3$ ** $(Ca_{0.29}Cd_{0.71})CO_3$	5040	8.43	0.323	0.094	0.733	−11.20	−11.17	−807.45	−807.26
	5760	8.56	0.330	0.081	0.800	−11.10	±0.07	−806.88	±0.38
	6480	8.53	0.322	0.064	0.804	−11.20		−807.45	
* $(Ca_{0.21}Cd_{0.79})CO_3$ ** $(Ca_{0.19}Cd_{0.81})CO_3$	5040	8.46	0.221	0.090	0.537	−11.69	−11.59	−762.65	−762.05
	5760	8.49	0.231	0.117	0.612	−11.52	±0.10	−761.68	±0.60
	6480	8.54	0.241	0.090	0.645	−11.55		−761.84	
* $(Ca_{0.11}Cd_{0.89})CO_3$ ** $(Ca_{0.10}Cd_{0.90})CO_3$	5040	8.36	0.140	0.231	0.424	−11.82	−11.81	−720.57	−720.48
	5760	8.38	0.140	0.228	0.455	−11.78	±0.03	−720.34	±0.14
	6480	8.48	0.142	0.170	0.448	−11.82		−720.52	

Table 2. Cont.

Sample	Dissolution Time (h)	pH	Concentration			# log IAP	Mean log IAP	ΔG_f^θ (kJ/mol)	Mean ΔG_f^θ (kJ/mol)
			Ca (mmol/L)	Cd (μ mol/L)	HCO ₃ +CO ₃ (mmol/L)				
(Ca _{0.00} Cd _{1.00})CO ₃	5040	7.83		5.320	0.149	−11.66	−11.62	−672.06	−671.81
	5760	7.84		5.435	0.155	−11.63	±0.05	−671.86	±0.29
	6480	7.83		6.476	0.152	−11.57		−671.52	
(Ca _{0.00} Cd _{1.00})CO ₃	5040	7.79		3.461	0.151	−11.89	−11.79	−673.33	−672.78
	5760	7.89		3.621	0.147	−11.78	±0.10	−672.70	±0.55
	6480	7.86		4.395	0.152	−11.71		−672.32	

Note: ^{a,b} Duplication; * Bulk component before dissolution; ** Bulk component after dissolution. # Calculated with respect to the bulk component after dissolution.

Table 3. Analytical data and solubility for the calcite–otavite solid solutions [(Ca_{1-x}Cd_x)CO₃] in the CO₂-saturated water at 25 °C.

Sample	Dissolution Time (h)	pH	Concentration			# log IAP	Mean log IAP	ΔG_f^θ (kJ/mol)	Mean ΔG_f^θ (kJ/mol)
			Ca (mmol/L)	Cd (μ mol/L)	HCO ₃ +CO ₃ (mmol/L)				
^a (Ca _{1.00} Cd _{0.00})CO ₃	5040	7.91	0.803		1.645	−8.47	−8.39	−1129.76	−1129.32
	5760	7.97	0.817		1.716	−8.38	±0.08	−1129.28	±0.44
	6480	8.05	0.801		1.668	−8.32		−1128.93	
^b (Ca _{1.00} Cd _{0.00})CO ₃	5040	7.90	0.825		1.741	−8.44	−8.37	−1129.62	−1129.22
	5760	7.93	0.853		1.776	−8.39	±0.09	−1129.33	±0.52
	6480	8.06	0.837		1.721	−8.28		−1128.70	
* (Ca _{0.90} Cd _{0.10})CO ₃	5040	7.90	0.774	0.074	1.896	−8.92	−8.88	−1075.24	−1075.02
	5760	7.89	0.822	0.046	2.023	−8.91	±0.06	−1075.17	±0.37
	6480	8.01	0.794	0.047	1.931	−8.82		−1074.65	
* (Ca _{0.79} Cd _{0.21})CO ₃	5040	7.87	0.877	0.051	2.097	−9.40	−9.38	−1020.85	−1020.74
	5760	7.87	0.870	0.068	2.092	−9.37	±0.02	−1020.70	±0.11
	6480	7.99	0.816	0.041	1.899	−9.36		−1020.65	
* (Ca _{0.69} Cd _{0.31})CO ₃	5040	7.82	0.889	0.111	2.202	−9.74	−9.70	−975.19	−975.01
	5760	7.85	0.922	0.101	2.196	−9.71	±0.04	−975.06	±0.23
	6480	8.02	0.885	0.063	2.005	−9.66		−974.78	
* (Ca _{0.60} Cd _{0.40})CO ₃	5040	7.83	0.938	0.132	2.001	−10.15	−10.13	−925.21	−925.07
	5760	7.83	0.916	0.123	2.053	−10.16	±0.06	−925.26	±0.32
	6480	7.98	0.902	0.103	1.964	−10.07		−924.75	
* (Ca _{0.50} Cd _{0.50})CO ₃	5040	7.83	0.932	0.192	1.884	−10.48	−10.53	−879.46	−879.74
	5760	7.82	0.880	0.148	1.933	−10.55	±0.05	−879.86	±0.28
	6480	7.92	0.853	0.103	1.878	−10.55		−879.90	
* (Ca _{0.40} Cd _{0.60})CO ₃	5040	7.83	0.837	0.137	1.856	−11.00	−10.98	−830.09	−830.00
	5760	7.87	0.842	0.129	1.870	−10.97	±0.02	−829.95	±0.09
	6480	8.03	0.803	0.082	1.780	−10.98		−829.97	
* (Ca _{0.30} Cd _{0.70})CO ₃	5040	7.84	0.875	0.161	1.936	−11.26	−11.26	−788.75	−788.72
	5760	7.88	0.902	0.131	1.950	−11.29	±0.04	−788.89	±0.19
	6480	7.99	0.865	0.129	1.796	−11.22		−788.53	
* (Ca _{0.21} Cd _{0.79})CO ₃	5040	7.86	0.763	0.374	1.691	−11.33	−11.47	−746.30	−747.10
	5760	7.85	0.789	0.210	1.702	−11.55	±0.14	−747.54	±0.80
	6480	7.96	0.771	0.174	1.606	−11.53		−747.47	
* (Ca _{0.11} Cd _{0.89})CO ₃	5040	7.94	0.481	0.463	1.051	−11.62	−11.64	−709.89	−710.00
	5760	7.94	0.462	0.416	1.054	−11.66	±0.02	−710.13	±0.13
	6480	8.04	0.458	0.363	1.014	−11.64		−709.99	
(Ca _{0.00} Cd _{1.00})CO ₃	5040	7.66		9.643	0.219	−11.42	−11.49	−670.66	−671.09
	5760	7.65		8.513	0.196	−11.53	±0.07	−671.29	±0.43
	6480	7.73		6.957	0.197	−11.53		−671.31	
(Ca _{0.00} Cd _{1.00})CO ₃	5040	7.65		6.894	0.214	−11.58	−11.60	−671.60	−671.71
	5760	7.65		6.023	0.201	−11.67	±0.07	−672.09	±0.38
	6480	7.75		6.636	0.186	−11.56		−671.45	

Note: ^{a,b} Duplication; * Bulk component before dissolution; ** Bulk component after dissolution. # Calculated with respect to the bulk component after dissolution.

For the dissolution in the N₂-degassed water at 25 °C, the mean solubility products (log K_{sp}) and the Gibbs free energies of formation (ΔG_f^θ) were estimated to be -8.45 ± 0.04 – -8.42 ± 0.06 and -1129.65 ± 0.22 – -1129.48 ± 0.30 kJ/mol for calcite [CaCO₃] and -11.62 ± 0.05 – -11.79 ± 0.10 and -671.81 ± 0.29 – -672.78 ± 0.55 kJ/mol for otavite [CdCO₃], respectively. For the dissolution in the CO₂-saturated water at 25 °C, the mean log K_{sp} and ΔG_f^θ values were estimated to be -8.39 ± 0.08 – -8.37 ± 0.09 and -1129.32 ± 0.44 – -1129.22 ± 0.52 kJ/mol for calcite [CaCO₃] and -11.49 ± 0.07 – -11.60 ± 0.07 and -671.09 ± 0.43 – -671.71 ± 0.38 kJ/mol for otavite [CdCO₃], respectively.

The results are consistent with the various K_{sp} and ΔG_f^θ values for CaCO_3 found in the literature. For instance, either the minteq.v4.dat database [35] or the phreeqc.dat database gives a $\log K_{sp}$ of -8.48 [26,36]. CaCO_3 has a very well-defined solubility product ($\log K_{sp}$) value between -8.30 [37] and -8.58 [38]. Many inconsistent values of the solubility product and ΔG_f^θ for otavite [CdCO_3] have been reported in the literature (Supplementary Material Tables S2 and S3). Some of the $\log K_{sp}$ values for otavite [CdCO_3] reported are: -13.74 [20]; -13.6 [39]; -12.1 ± 0.1 [2]; -12.06 [40]; -12.03 ± 0.13 [41]; -11.31 ± 0.03 [23]; -11.292 [42]; -11.284 [43] and -11.209 [44]. The various ΔG_f^θ values for otavite [CdCO_3] found in the literature ranged from -595.07 ± 4.18 kJ/mol [45] to -779.43 kJ/mol [46], including -662.7 kJ/mol [21]; -669.44 ± 2.64 kJ/mol [47]; -670.3 ± 2.1 kJ/mol [48]; -671.1 ± 1.1 [49]; -672.79 kJ/mol [43]; -674.2 ± 0.6 kJ/mol [50]; -674.7 ± 0.6 kJ/mol [2] and -683.46 kJ/mol [39]. As a result, a great difference among the $\log K_{sp}$ values for otavite [CdCO_3] could be also found in various databases. For instance, whereas the minteq.v4.dat database [35] compiles a $\log K_{sp}$ of -12.0 , the wateq4f.dat database gives a $\log K_{sp}$ of -12.1 and the llnl.dat database gives a $\log K_{sp}$ of -12.2288 [26,36].

For the dissolution in the N_2 -degassed water, with the increasing X_{Cd} of the $(\text{Ca}_{1-x}\text{Cd}_x)\text{CO}_3$ solid solution, $\log K_{sp}$ values decreased non-linearly from -8.45 ± 0.04 – -8.42 ± 0.06 for calcite [CaCO_3] to -11.62 ± 0.05 – -11.79 ± 0.10 for otavite [CdCO_3] (Supplementary Material Figure S6), while the estimated ΔG_f^θ values increased linearly from -1129.65 ± 0.22 – -1129.48 ± 0.30 kJ/mol for calcite to -671.81 ± 0.29 – -672.78 ± 0.55 kJ/mol for otavite (Supplementary Material Figure S7). For the dissolution in the CO_2 -saturated water, with the increasing X_{Cd} , the $\log K_{sp}$ values decreased non-linearly from -8.39 ± 0.08 – -8.37 ± 0.09 for calcite [CaCO_3] to -11.49 ± 0.07 – -11.60 ± 0.07 for otavite [CdCO_3] (Supplementary Material Figure S6), while the estimated ΔG_f^θ values increased linearly from -1129.32 ± 0.44 – -1129.22 ± 0.52 kJ/mol for calcite to -671.09 ± 0.43 – -671.71 ± 0.38 kJ/mol for otavite (Supplementary Material Figure S7). These results were in close agreement with the experimental points and the straight line which connects the $\log K_{sp}$ values for CaCO_3 and CdCO_3 , the endmembers of the solid solution series [9]. The $\Delta G_f^\theta[(\text{Ca}_{1-x}\text{Cd}_x)\text{CO}_3]$ values were estimated to vary nearly linearly from -1128.79 kJ/mol for calcite to -671.06 kJ/mol for otavite with mineral composition for miscible solids [49]. Complete miscibility is consistent with the similarity in ionic radii of the two metals; the ionic radii of Ca^{2+} and Cd^{2+} in octahedral coordination to oxygens are 0.99 Å and 0.97 Å, respectively, and the endmember phases otavite and calcite are isomorphous.

3.4. Lippmann Diagram

3.4.1. Construction of the Lippmann Diagram

The solid solution–aqueous solution (SSAS) system is fundamentally important in understanding the geochemical interaction. The construction method for the Lippmann diagrams involving several SSAS systems have been depicted in detail by many previous works [11,22,24,28,51–54].

The Lippmann diagram is a chart that displays the relationship between the “solidus” and “solutus” phases in the SSAS system. The “total activity product” ($\Sigma\Pi_{SS}$) is expressed by the sum of the partial activity products of the two endmembers at equilibrium. The “solidus” curve and the “solutus” curve are the plotting of $\Sigma\Pi_{SS}$ against the solid component and the solution component, respectively.

For the calcite–otavite solid solutions [$(\text{Ca}_{1-x}\text{Cd}_x)\text{CO}_3$], the “solidus” curve is defined as:

$$\Sigma\Pi_{SS} = \left(\{ \text{Ca}^{2+} \} + \{ \text{Cd}^{2+} \} \right) \{ \text{CO}_3^{2-} \} = K_{\text{Ca}} X_{\text{Ca}} \gamma_{\text{Ca}} + K_{\text{Cd}} X_{\text{Cd}} \gamma_{\text{Cd}} \quad (12)$$

where $\{ \}$ represents aqueous activity. K_{Ca} and K_{Cd} , X_{Ca} and X_{Cd} , γ_{Ca} and γ_{Cd} are the solubility products, the mole ratios ($1-x$, x) and the activity coefficients of CaCO_3 and CdCO_3 in the $(\text{Ca}_{1-x}\text{Cd}_x)\text{CO}_3$ solid solutions, respectively.

The “solutus” curve is defined as:

$$\Sigma\Pi_{SS} = \frac{1}{\frac{X_{Ca^{2+},aq}}{K_{Cd}\gamma_{Ca}} + \frac{X_{Cd^{2+},aq}}{K_{Cd}\gamma_{Cd}}} \quad (13)$$

where $X_{Ca^{2+},aq}$ and $X_{Cd^{2+},aq}$ are the activity ratios of the aqueous free ions of Ca^{2+} and Cd^{2+} .

For the members of fixed X_{Cd} , a series of the minimum stoichiometric saturation curves are defined as:

$$\Sigma\Pi_{SS} = \frac{IAP}{(X_{Ca^{2+},aq})^{X_{Ca}}(X_{Cd^{2+},aq})^{X_{Cd}}} \quad (14)$$

The saturation curves for the two endmembers, pure $CaCO_3$ and $CdCO_3$, are defined as:

$$\Sigma\Pi_{CaCO_3} = \frac{\{Ca^{2+}\}\{CO_3^{2-}\}}{(X_{Ca^{2+},aq})^{X_{Ca}}} = \frac{K_{Ca}}{(X_{Ca^{2+},aq})^{X_{Ca}}} \quad (15)$$

$$\Sigma\Pi_{CdCO_3} = \frac{\{Cd^{2+}\}\{CO_3^{2-}\}}{(X_{Cd^{2+},aq})^{X_{Cd}}} = \frac{K_{Cd}}{(X_{Cd^{2+},aq})^{X_{Cd}}} \quad (16)$$

3.4.2. Lippmann Diagram for the Non-Ideal $(Ca_{1-x}Cd_x)CO_3$ Solid Solutions

The Lippmann diagram for the $(Ca_{1-x}Cd_x)CO_3$ solid solutions has been calculated by using the endmembers $\log K_{sp}$ values of -8.48 for calcite [36] and -12.1 for otavite [2] and assuming an ideal solid solution [11]. The extremely low solubility of otavite compared to calcite indicates a great preferential partitioning of $CdCO_3$ in the solids [55] and explains the effectiveness of carbonates in eliminating cadmium from the environments [10,12,15,17,22,23]. A small variation of $X_{Cd,aq}$ results in a big change of the X_{Cd} in the solid. Only a very limited range of the aqueous composition can exist in equilibrium with the intermediate solid solution [11]. The solid tends to be either Ca-rich ($X_{Cd} < 0.1$) or Cd-rich ($X_{Cd} > 0.9$) in a very narrow range of the fluid composition ($0.000027 < X_{Cd,aq} < 0.002154$) [11].

Previous experiments have revealed that a regular model was perhaps inadequate to illustrate closely thermodynamic equilibria involving carbonates [56]. The sub-regular model (two-parameter Guggenheim equation) could be more successfully employed to fit experimental solubility data for the $(Ca,Mg)CO_3-H_2O$, $(Sr,Ba)CO_3-H_2O$, $(Sr,Ca)CO_3-H_2O$ systems [52]. In defect of more exact data, thus, the two Guggenheim coefficients a_0 and a_1 were estimated in the present work, assuming the $(Ca_{1-x}Cd_x)CO_3$ solid solutions to be sub-regular.

When the SSAS interaction achieved the stoichiometric saturation state, the two Guggenheim parameters a_0 and a_1 can be estimated by using:

$$\ln K_{sp} = x(1-x)a_0 + x(1-x)(x-(1-x))a_1 + (1-x)\ln[(1-x)K_{Ca}] + x\ln[xK_{Cd}] \quad (17)$$

The \log IAPs ($\approx \log K_{sp}$) for the last three solution samples after 5040–6480 h dissolution in the N_2 -degassed water and the CO_2 -saturated pure water are plotted against X_{Cd} of the $(Ca_{1-x}Cd_x)CO_3$ solid solutions (Supplementary Material Figure S8), which exhibited that the experimental $\log K_{sp}$ values were close to and somewhat lower than the data for ideal $(Ca_{1-x}Cd_x)CO_3$ solid solutions. The K_{sp} values as a function of X_{Cd} could be very well fitted to Equation (17) with the two-parameter Guggenheim equations of $a_0 = -0.84$ and $a_1 = -3.80$, $a_0 = -1.12$ and $a_1 = -3.83$, respectively.

3.4.3. Solid Solution–Aqueous Solution Interaction

Figures 7 and 8 illustrate the Lippmann diagrams for the $(Ca_{1-x}Cd_x)CO_3$ solid solutions at $25^\circ C$, which were computed with the sub-regular solid solution (a_0 and a_1) and the endmember $\log K_{sp}$ values for calcite [$CaCO_3$] and otavite [$CdCO_3$] from the results of dissolution in the N_2 -degassed water and the CO_2 -saturated water, respectively. Along

with the *solutus* curve and the *solidus* curve, the stoichiometric saturation curves for pure calcite ($X_{Cd} = 0.00$), the $(Ca_{1-x}Cd_x)CO_3$ solid solutions ($X_{Cd} = 0.21, 0.41, 0.61$ and 0.81) and pure otavite ($X_{Cd} = 1.00$) were also calculated and drawn in the Lippmann diagrams.

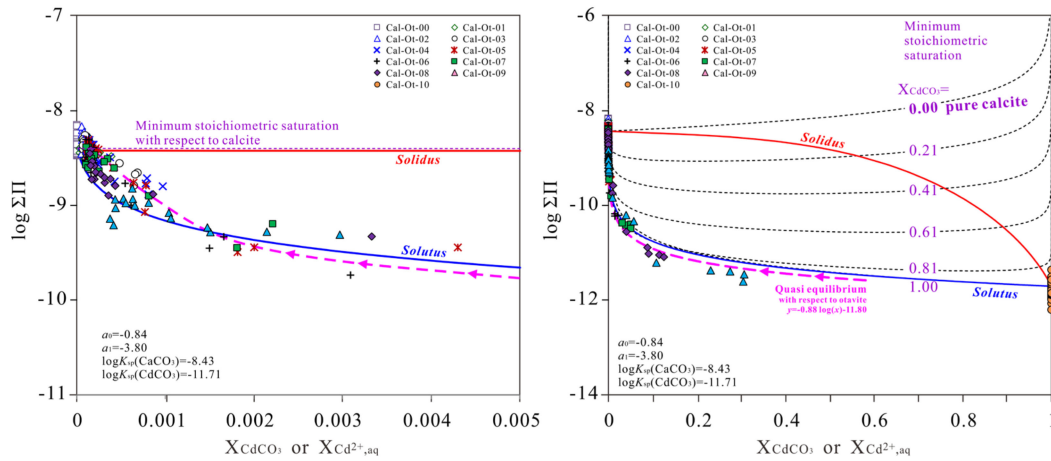


Figure 7. Lippmann diagram for the non-ideal $(Ca_{1-x}Cd_x)CO_3$ solid solutions together with the plot of some stoichiometric saturation curves and the experimental data for dissolution in the N_2 -degassed water. The graph on the left is a zoom of the one on the right.

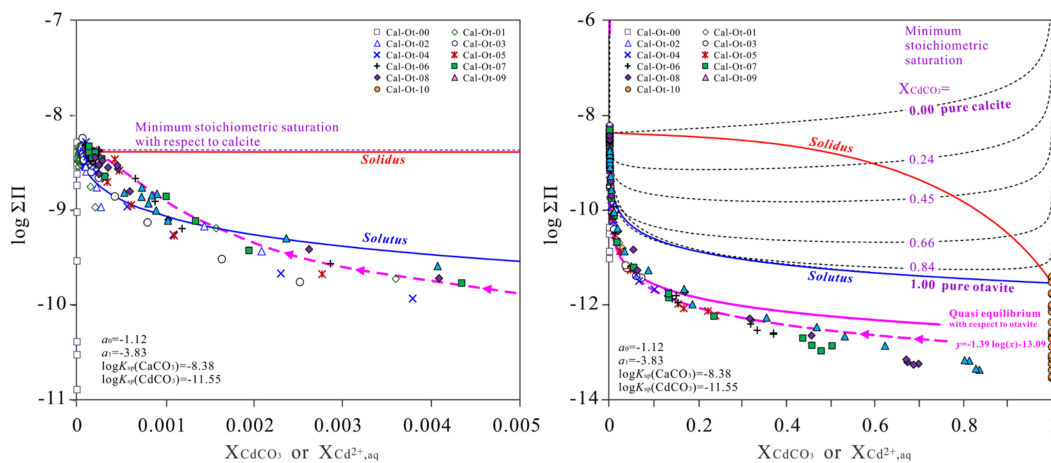


Figure 8. Lippmann diagram for the non-ideal $(Ca_{1-x}Cd_x)CO_3$ solid solutions together with the plot of some stoichiometric saturation curves and the experimental data for dissolution in the CO_2 -saturated water. The graph on the left is a zoom of the one on the right.

The curve for the saturation with respect to otavite and the *solutus* curve closely follow each other except in the part where $X_{Cd,aq}$ is approximate to 0.00, in which the pure otavite saturation curve approaches an infinitely great $\Sigma\Pi$ value, while the *solutus* curve intercepts the $\Sigma\Pi$ axis when the value is equal to the pure calcite solubility product. The pure calcite saturation curve is always above the *solutus* curve (except at $X_{CaCO_3} = 1.00$); hence, all solutions at thermodynamic equilibrium with respect to any $(Ca_{1-x}Cd_x)CO_3$ solids are always unsaturated with respect to pure calcite. These solutions are also always unsaturated with respect to pure otavite by an extremely small degree. Since the K_{sp} value for calcite is greatly larger than that of otavite, the *solutus* curve will fundamentally be identical to the pure otavite saturation curve when the solid-solution activity coefficient is unity except at the $X_{Cd,aq}$ value very close to zero.

The quasi-equilibrium is the state when the thermodynamic equilibrium is not attained [57], but the driving force for the ion flux of one or both components between aqueous solution and solid solution can be negligible, and one of the two chemical poten-

tial differences is zero, but the other is not. At the fixed X_{Cd} of the $(Ca_{1-x}Cd_x)CO_3$ solid solutions, $\Sigma\Pi_{Cd}$ with respect to otavite is expressed as a function of $X_{Cd,aq}$:

$$\Sigma\Pi_{Cd}(X_{Cd^{2+},aq}) = [K_{Cd}\gamma_{Cd}X_{Cd}]/[X_{Cd^{2+},aq}] \quad (18)$$

The solid rose lines in the Lippmann diagrams showed the quasi-equilibrium of the solid solution of $X_{Cd} = 0.10$ with respect to the whole series of aqueous solutions (Figures 7 and 8). The region under the solid rose lines denoted unsaturation with respect to $CdCO_3$ and $CaCO_3$; the region above the solid rose lines denoted oversaturation with respect to $CdCO_3$ and unsaturation with respect to $CaCO_3$.

In addition, the data of this work were also plotted as $(\{Ca^{2+}\} + \{Cd^{2+}\})\{CO_3^{2-}\}$ versus $X_{Cd^{2+},aq}$ for dissolution in the N_2 -degassed water (Figure 7) and the CO_2 -saturated pure waters (Figure 8). An increase in the released Ca^{2+} concentration and a highest Cd^{2+} concentration for the solids were generally viewed in the dissolution progress. The experimental data points indicated that the $(Ca_{1-x}Cd_x)CO_3$ solid solutions dissolved incongruently and moved progressively up to the quasi-equilibrium curve for otavite [$CdCO_3$] and then along the quasi-equilibrium curve for otavite from right to left, approached the *solutus* curve and finally reached the minimum stoichiometric saturation for calcite [$CaCO_3$]. The aqueous Cd-poor solutions were finally in equilibrium with the $CdCO_3$ -rich solids. The saturation indexes (SI) with respect to otavite [$CdCO_3$] increased as X_{Cd} increased, and the aqueous solutions were unsaturated with respect to otavite throughout the dissolution of the solid solution in the CO_2 -saturated water, indicating that the dissolution of the calcite–otavite solid solutions [$(Ca_{1-x}Cd_x)CO_3$] might be controlled by a quasi-equilibrium with respect to otavite (Figures 7 and 8; Supplementary Material Figure S9). The dissolution of a solid solution to stoichiometric saturation would cause either oversaturation or unsaturation with respect to the pure endmembers [25]. In the SSAS system for $(Ca_{1-x}Cd_x)CO_3$, oversaturation is expected with respect to the $CdCO_3$ endmember if the mole fraction of $CdCO_3$ in the solid solution is greater than $\approx 10^{-2.75}$ [25]. The extremely great difference between the calcite and otavite solubility products decided that the *solidus* curve and the *solutus* curve plot very far apart. Thus, the compositions of the aqueous and solid phases coexisting at equilibrium differed extremely, i.e., a considerably Cd-poor aqueous solution might be in equilibrium with a considerably Cd-rich solid phase. These results offer a deeper understanding of the geochemical cycle of cadmium in the environment.

4. Conclusions

For the dissolution of the calcite–otavite solid solutions [$(Ca_{1-x}Cd_x)CO_3$] in the N_2 -degassed water, the Ca concentrations of the aqueous phases increased up to the steady states after 5040 h of dissolution and the Cd concentrations of the aqueous phases increased up to the highest values and then decreased gradually to the steady states of 0.017–6.476 $\mu\text{mol/L}$ after 5040 h of dissolution. For the dissolution in the CO_2 -saturated water, the Ca and Cd concentrations of the aqueous phases increased up to the highest value and then decreased gradually to the steady states of 0.94–0.46 mmol/L and 0.046–9.643 $\mu\text{mol/L}$ after 5040 h of dissolution, respectively. The $Cd/(Ca+Cd)$ mole ratios of the aqueous phases were obviously smaller than the $Cd/(Ca+Cd)$ mole ratios of the corresponding solid phases and decreased with time to the steady states, indicating a strong non-stoichiometric release of Ca and Cd.

For the dissolution in the N_2 -degassed and CO_2 -saturated pure waters at 25 °C, the mean log IAP values at the longstanding steady state ($\approx \log K_{sp}$) were estimated for calcite [$CaCO_3$] to be -8.45 ± 0.04 – -8.42 ± 0.06 and -8.39 ± 0.08 – -8.37 ± 0.09 with the ΔG_f^θ values of -1129.65 ± 0.22 – -1129.48 ± 0.30 kJ/mol and -1129.32 ± 0.44 – -1129.22 ± 0.52 kJ/mol , respectively. For the dissolution in the N_2 -degassed and CO_2 -saturated pure waters at 25 °C, the mean log IAP values at the longstanding steady state ($\approx \log K_{sp}$) were estimated for otavite [$CdCO_3$] to be -11.62 ± 0.05 – -11.79 ± 0.10 and -11.49 ± 0.07 – -11.60 ± 0.07 with the ΔG_f^θ values of -671.81 ± 0.29 – -672.78 ± 0.55 kJ/mol and

-671.09 ± 0.43 — -671.71 ± 0.38 kJ/mol, respectively. Generally, the log IAP values at the final longstanding steady states decreased non-linearly, and the estimated ΔG_f^θ values increased linearly with the increasing X_{Cd} of the $(Ca_{1-x}Cd_x)CO_3$ solid solution.

In the Lippmann diagrams constructed for the sub-regular $(Ca_{1-x}Cd_x)CO_3$ solid solutions with the estimated Guggenheim coefficients $a_0 = -0.84$ and $a_1 = -3.80$ or $a_0 = -1.12$ and $a_1 = -3.83$, the $(Ca_{1-x}Cd_x)CO_3$ solid solutions dissolved incongruently, moved progressively up to the quasi-equilibrium curve for otavite [$CdCO_3$], and then along the quasi-equilibrium curves for otavite from right to left, approached the *solutus* curves and finally reached the minimum stoichiometric saturation curves for calcite [$CaCO_3$]. The dissolution of the calcite–otavite solid solutions [$(Ca_{1-x}Cd_x)CO_3$] might be controlled by a quasi-equilibrium with respect to otavite. The considerably Cd-poor aqueous phases were finally in equilibrium with the $CdCO_3$ -rich solid phases.

Supplementary Materials: The following supporting information can be downloaded at: <https://www.mdpi.com/article/10.3390/min12060756/s1>, Table S1: Speciation reaction in the PHREEQC simulation; Table S2: Solubility constants (log K) of otavite at standard state; Table S3: Gibbs free energies of formation (ΔG_f^θ) of otavite; Figure S1: Position variation of the strongest peak (104) with the solid composition X_{Cd} : (a) before dissolution, and (b) after dissolution in the N_2 -degassed water for 270 d and (c) after dissolution in the CO_2 -saturated water for 270 d; Figure S2: SEM image of the $(Ca_{1-x}Cd_x)CO_3$ solid solutions before dissolution; Figure S3: SEM image of calcite (Cal-Ot-00) after dissolution for 270 d; Figure S4: Change of the Cd/(Ca+Cd) mole ratios of the aqueous phases during the dissolution of the $(Ca_{1-x}Cd_x)CO_3$ solid solution; Figure S5: Variation of the final aqueous phases with the solid X_{Cd} mole ratios during the dissolution of the $(Ca_{1-x}Cd_x)CO_3$ solid solutions in water; Figure S6: Change of log IAP ($\approx \log K_{sp}$) for the $(Ca_{1-x}Cd_x)CO_3$ solid solution with the $CdCO_3$ mole fraction (X_{CdCO_3}); Figure S7: Change of the Gibbs free energy of formation (ΔG_f^θ) for the $(Ca_{1-x}Cd_x)CO_3$ solid solution with the $CdCO_3$ mole fraction (X_{CdCO_3}); Figure S8: Estimation of the Guggenheim coefficients (a_0 and a_1) for the non-ideal $(Ca_{1-x}Cd_x)CO_3$ solid solution; Figure S9: Saturation index of the aqueous solution with respect to calcite and otavite during the dissolution of the $(Ca_{1-x}Cd_x)CO_3$ solid solution.

Author Contributions: Conceptualization, Y.Z.; Data curation, H.Y., C.M. and P.N.; Formal analysis, H.Y., P.N. and F.X.; Funding acquisition, Y.Z.; Investigation, C.M. and S.T.; Methodology, C.M.; Project administration, Y.Z.; Visualization, Z.Z. and Y.Z.; Writing—Original draft, Y.Z.; Writing—Review and Editing, Z.Z., L.Z. and Z.K. All authors have read and agreed to the published version of the manuscript.

Funding: The present research was funded by the National Natural Science Foundation of China (42063003) and the Science & Technology Planning Projects of Guangxi (2018GXNSFAA050044).

Data Availability Statement: Not applicable.

Acknowledgments: The manuscript has greatly benefited from insightful comments by editors and three anonymous reviewers. The authors would like to acknowledge the Science and Education Combined with Science and Technology Innovation Base of Guangxi Key Laboratory of Environmental Pollution Control Theory and Technology for the help in solid and solution analysis.

Conflicts of Interest: The authors declare no conflict of interest.

References

1. Pérez-Garrido, C.; Fernández-Díaz, L.; Pina, C.M.; Prieto, M. In situ AFM observations of the interaction between calcite (10 $\bar{1}$ 4) surfaces and Cd-bearing aqueous solutions. *Surf. Sci.* **2007**, *601*, 5499–5509. [[CrossRef](#)]
2. Stipp, S.L.; Parks, G.A.; Nordstrom, D.K.; Leckie, J.O. Solubility-product constant and thermodynamic properties for synthetic otavite, $CdCO_{3(s)}$, and aqueous association constants for the Cd(II)- CO_2 - H_2O system. *Geochim. Cosmochim. Acta* **1993**, *57*, 2699–2713. [[CrossRef](#)]
3. Katsikopoulos, D.; Fernández-González, A.; Prieto, M. Crystallization of the $(Cd,Ca)CO_3$ solid solution in double diffusion systems: The partitioning behaviour of Cd^{2+} in calcite at different supersaturation rates. *Mineral. Mag.* **2008**, *72*, 433–436. [[CrossRef](#)]
4. Ma, Y.; Ran, D.; Shi, X.; Zhao, H.; Liu, Z. Cadmium toxicity: A role in bone cell function and teeth development. *Sci. Total Environ.* **2021**, *769*, 144646. [[CrossRef](#)] [[PubMed](#)]

5. Sasamoto, R.; Kanda, Y.; Yamanaka, S. Difference in cadmium chemisorption on calcite and vaterite porous particles. *Chemosphere* **2022**, *297*, 134057. [[CrossRef](#)] [[PubMed](#)]
6. Wen, Y.B.; Li, W.; Yang, Z.F.; Zhang, Q.Z.; Ji, J.F. Enrichment and source identification of Cd and other heavy metals in soils with high geochemical background in the karst region, Southwestern China. *Chemosphere* **2019**, *245*, 125620. [[CrossRef](#)] [[PubMed](#)]
7. Xia, X.; Ji, J.; Yang, Z.; Han, H.; Huang, C.; Li, Y.; Zhang, W. Cadmium risk in the soil-plant system caused by weathering of carbonate bedrock. *Chemosphere* **2020**, *254*, 126799. [[CrossRef](#)] [[PubMed](#)]
8. Yaciuk, P.A.; Colombo, F.; Lecomte, K.L.; De Micco, G.; Bohé, A.E. Cadmium sources, mobility, and natural attenuation in contrasting environments (carbonate-rich and carbonate-poor) in the Capillitas polymetallic mineral deposit, NW Argentina. *Appl. Geochem.* **2022**, *136*, 105152. [[CrossRef](#)]
9. Papadopoulos, P.; Rowell, D.L. The reactions of cadmium with calcium carbonate surfaces. *Eur. J. Soil Sci.* **1988**, *39*, 23–36. [[CrossRef](#)]
10. Chiarello, R.P.; Sturchio, N.C.; Grace, J.D.; Geissbuhler, P.; Sorensen, L.B.; Cheng, L.; Xu, S. Otavite-calcite solid-solution formation at the calcite-water interface studied in situ by synchrotron X-ray scattering. *Geochim. Cosmochim. Acta* **1997**, *61*, 1467–1474. [[CrossRef](#)]
11. Prieto, M.; Fernández-González, A.; Putnis, A.; Fernández-Díaz, L. Nucleation, growth, and zoning phenomena in crystallizing (Ba,Sr)CO₃, Ba(SO₄,CrO₄), (Ba,Sr)SO₄, and (Cd,Ca)CO₃ solid solutions from aqueous solutions. *Geochim. Cosmochim. Acta* **1997**, *61*, 3383–3397. [[CrossRef](#)]
12. Prieto, M.; Cubillas, P.; Fernández-González, A. Uptake of dissolved Cd by biogenic and abiogenic aragonite: A comparison with sorption onto calcite. *Geochim. Cosmochim. Acta* **2003**, *67*, 3859–3869. [[CrossRef](#)]
13. Cubillas, P.; Köhler, S.; Prieto, M.; Causserand, C.; Oelkers, E.H. How do mineral coatings affect dissolution rates? An experimental study of coupled CaCO₃ dissolution—CdCO₃ precipitation. *Geochim. Cosmochim. Acta* **2005**, *69*, 5459–5476. [[CrossRef](#)]
14. Li, Z.; Hofmann, A.; Wolthers, M.; Thomas, P. Reversibility of cadmium sorption to calcite revisited. *J. Colloid Interf. Sci.* **2012**, *368*, 434–442. [[CrossRef](#)]
15. Tesoriero, A.J.; Pankow, J.F. Solid solution partitioning of Sr²⁺, Ba²⁺ and Cd²⁺ to calcite. *Geochim. Cosmochim. Acta* **1996**, *60*, 1053–1063. [[CrossRef](#)]
16. Königsberger, E.; Hausner, R.; Gamsjäger, H. Solid-solute equilibria in aqueous solution: V. The system CdCO₃-CaCO₃-CO₂-H₂O. *Geochim. Cosmochim. Acta* **1991**, *55*, 3505–3514. [[CrossRef](#)]
17. Stipp, S.L.; Hochella, M.F.; Parks, G.A.; Leckie, J.O. Cd²⁺ uptake by calcite, solid-state diffusion, and the formation of solid-solution: Interface processes observed with near-surface sensitive techniques (XPS, LEED, and AES). *Geochim. Cosmochim. Acta* **1992**, *56*, 1941–1954. [[CrossRef](#)]
18. Reeder, R.J. Interaction of divalent cobalt, zinc, cadmium, and barium with the calcite surface during layer growth. *Geochim. Cosmochim. Acta* **1996**, *60*, 1543–1552. [[CrossRef](#)]
19. Wang, Q.; De Leeuw, N.H. A computer-modelling study of CdCO₃-CaCO₃ solid solutions. *Mineral. Mag.* **2008**, *72*, 525–529. [[CrossRef](#)]
20. Smith, R.M.; Martell, A.E. *Critical Stability Constants, Volume 4, Inorganic Complexes*; Plenum Press: New York, NY, USA, 1976; pp. 1–257.
21. Sverjensky, D.A. Prediction of Gibbs free energies of calcite type carbonates and the equilibrium distribution of trace elements between carbonates and aqueous solutions. *Geochim. Cosmochim. Acta* **1984**, *48*, 1127–1134. [[CrossRef](#)]
22. Prieto, M. Thermodynamics of solid solution aqueous solution systems. *Rev. Mineral. Geochem.* **2009**, *70*, 47–85. [[CrossRef](#)]
23. Davis, J.A.; Fuller, C.C.; Cook, A.S. A model for trace metal sorption processes at the calcite surface: Adsorption of Cd²⁺ and subsequent solid solution formation. *Geochim. Cosmochim. Acta* **1987**, *51*, 1477–1490. [[CrossRef](#)]
24. Glynn, P.D.; Reardon, E.J. Solid-solution aqueous-solution equilibria: Thermodynamic theory and representation. *Amer. J. Sci.* **1990**, *290*, 164–201. [[CrossRef](#)]
25. Glynn, P. Solid-solution solubilities and thermodynamics: Sulfates, carbonates and halides. *Rev. Mineral. Geochem.* **2000**, *40*, 481–511. [[CrossRef](#)]
26. Parkhurst, D.L.; Appelo, C.A.J. *Description of Input and Examples for PHREEQC Version 3, A Computer Program for Speciation, Batch-Reaction, One-Dimensional Transport, and Inverse Geochemical Calculations*; Techniques and Methods, Book 6, Chapter A43; U.S. Geological Survey: Denver, CO, USA, 2013; pp. 1–497.
27. Astilleros, J.M.; Pina, C.M.; Fernández-Díaz, L.; Putnis, A. Molecular-scale surface processes during the growth of calcite in the presence of manganese. *Geochim. Cosmochim. Acta* **2002**, *66*, 3177–3189. [[CrossRef](#)]
28. Katsikopoulos, D.; Fernández-González, Á.; Prieto, M. Crystallization behaviour of the (Mn,Ca)CO₃ solid solution in silica gel: Nucleation, growth and zoning phenomena. *Mineral. Mag.* **2009**, *73*, 269–284. [[CrossRef](#)]
29. Putnis, A.; Prieto, M.; Fernández-González, L. Fluid supersaturation and crystallization in porous media. *Geol. Mag.* **1995**, *132*, 1–13. [[CrossRef](#)]
30. Fernández-Díaz, L.; Astilleros, J.M.; Pina, C.M. The morphology of calcite crystals grown in a porous medium doped with divalent cations. *Chem. Geol.* **2006**, *225*, 314–321. [[CrossRef](#)]
31. Alkattan, M.; Oelkers, E.H.; Dandurand, J.-L.; Schott, J. An experimental study of calcite and limestone dissolution rates as a function of pH from −1 to 3 and temperature from 25 to 80 °C. *Chem. Geol.* **1998**, *151*, 199–214. [[CrossRef](#)]

32. Zhang, X.; Wu, S.; Chen, F. Nano precipitates formed during the dissolution of calcite incorporated with Cu and Mn. *Minerals* **2018**, *8*, 484. [[CrossRef](#)]
33. Mucci, A. The behavior of mixed Ca-Mn carbonates in water and seawater: Controls of manganese concentrations in marine porewaters. *Aquat. Geochem.* **2004**, *10*, 139–169. [[CrossRef](#)]
34. Stumm, W.; Morgan, J.J. *Aquatic Chemistry, Chemical Equilibria and Rates in Natural Waters*, 3rd ed.; John Wiley & Sons, Inc.: New York, NY, USA, 1996; pp. 976–1004.
35. Allison, J.D.; Brown, D.S.; Novo-Gradac, K.J. *MINTEQA2/PRODEFA2, a Geochemical Assessment Model for Environmental Systems: Version 3.0 User's Manual*; Environmental Research Laboratory, Office of Research and Development, U.S. Environmental Protection Agency: Athens, GA, USA, 1991; pp. 1–106.
36. Plummer, L.N.; Busenberg, E. The solubilities of calcite, aragonite and vaterite in CO₂-H₂O solutions between 0 and 90 °C, and an evaluation of the aqueous model for the system CaCO₃-CO₂-H₂O. *Geochim. Cosmochim. Acta* **1982**, *46*, 1011–1040. [[CrossRef](#)]
37. Garrels, R.M.; Thompson, M.E.; Siever, R. Stability of some carbonates at 25 °C and one atmosphere total pressure. *Am. J. Sci.* **1960**, *258*, 402–418. [[CrossRef](#)]
38. Jensen, D.L.; Boddum, J.K.; Tjell, J.C.; Christensen, T.H. The solubility of rhodochrosite (MnCO₃) and siderite (FeCO₃) in anaerobic aquatic environments. *Appl. Geochem.* **2002**, *17*, 503–511. [[CrossRef](#)]
39. Zhuk, N.P. Thermodynamic constants of sulfates, carbonates, chromates, bromates, iodates, oxalates, and other salts slightly soluble in water. *Zhurnal Fizicheskoi Khimii* **1954**, *28*, 1690–1697.
40. Krestov, G.A.; Kobenin, V.A.; Sokolov, V.N. Method for calculating the solubility product at 273–373 °K. *Zhurnal Neorg. Khimii* **1977**, *22*, 2864–3867.
41. Gamsjäger, H.; Magalhães, M.C.F.; Königsberger, E.; Sawada, K.; Churagulov, B.R.; Schmidt, P.; Zeng, D. IUPAC-NIST Solubility Data Series. 92. Metal Carbonates. Part 1. Solubility and related thermodynamic quantities of cadmium (II) carbonate in aqueous systems. *J. Phys. Chem. Ref. Data* **2011**, *40*, 043104.
42. Egorov, A.M.; Titova, Z.P. Solubility products of salts with polyatomic ions as a function of the temperature. *Zhurnal Neorg. Khimii* **1962**, *7*, 275–278.
43. Latimer, W.M. *The Oxidation States of the Elements and their Potentials in Aqueous Solutions*, 2nd ed.; Prentice Hall: New York, NY, USA, 1952; pp. 1–392.
44. Wagman, D.D.; Evans, W.H.; Parker, V.B.; Schumm, R.H.; Halow, I.; Bailey, S.M.; Churney, K.L.; Nuttall, R.L. The NBS tables of chemical thermodynamic properties: Selected values for inorganic and C1 and C2 organic substances in SI units. *J. Phys. Chem. Ref. Data* **1982**, *11* (Suppl. S2), 1–392.
45. Robie, R.A. *Thermodynamic Properties of Minerals*; Open File Report TEI-816; U.S. Geological Survey: Denver, CO, USA, 1962; pp. 1–31.
46. Barin, I.; Knacke, O.; Kubaschewski, O. *Thermodynamic Properties of Inorganic Substances, Supplement*; Springer: Berlin, Germany, 1977; pp. 1–861.
47. Robie, R.A.; Hemingway, B.S.; Fisher, J.R. *Thermodynamic Properties of Minerals and Related Substances at 298.15 K and 1 bar (10⁵ Pa) Pressure and at Higher Temperatures*; U.S. Geological Survey Bulletin 1452; U.S. Government Printing Office: Washington, DC, USA, 1978; pp. 1–456.
48. La Iglesia, A.; Félix, J.F. Estimation of thermodynamic properties of mineral carbonates at high and low temperatures from the sum of polyhedral contributions. *Geochim. Cosmochim. Acta* **1994**, *58*, 3983–3991. [[CrossRef](#)]
49. Rock, P.A.; Casey, W.H.; McBeath, M.K.; Walling, E.M. A new method for determining Gibbs energies of formation of metal-carbonate solid solutions: 1. The Ca_xCd_{1-x}CO_{3(s)} system at 298 K and 1 bar. *Geochim. Cosmochim. Acta* **1994**, *58*, 4281–4291. [[CrossRef](#)]
50. Gamsjäger, H.; Preis, W.; Königsberger, E.; Magalhaes, M.C.; Brandao, P. Solid-solute phase equilibria in aqueous solution. XI. Aqueous solubility and standard Gibbs energy of cadmium carbonate. *J. Solution Chem.* **1999**, *28*, 711–720. [[CrossRef](#)]
51. Lippmann, F. Phase diagrams depicting the aqueous solubility of binary mineral systems. *N. Jahrb. Mineral. Abh.* **1980**, *139*, 1–25.
52. Glynn, P.D.; Reardon, E.J.; Plummer, L.N.; Busenberg, E. Reaction paths and equilibrium end-points in solid-solution aqueous-solution systems. *Geochim. Cosmochim. Acta* **1990**, *54*, 267–282. [[CrossRef](#)]
53. Gamsjäger, H.; Königsberger, E.; Preis, W. Lippmann diagrams: Theory and application to carbonate systems. *Aquat. Geochem.* **2000**, *6*, 119–132. [[CrossRef](#)]
54. Fernández-González, A.; Pedreira, V.B.; Prieto, M. Crystallization of zoned (Ba,Pb)SO₄ single crystals from aqueous solution in silica gel. *J. Cryst. Growth* **2008**, *310*, 4616–4622. [[CrossRef](#)]
55. Fernández-González, A.; Prieto, M.; Putnis, A.; López Andrés, S. Concentric zoning patterns in crystallizing (Cd,Ca)CO₃ solid-solutions from aqueous solutions. *Miner. Mag.* **1999**, *63*, 331–343. [[CrossRef](#)]
56. McBeath, M.K.; Rock, P.A.; Casey, W.H.; Mandell, G.K. Gibbs energies of formation of metal-carbonate solid solutions: Part 3. The Ca_xMn_{1-x}CO₃ system at 298 K and 1 bar. *Geochim. Cosmochim. Acta* **1998**, *62*, 2799–2808. [[CrossRef](#)]
57. Shtukenberg, A.G.; Punin, Y.O.; Azimov, P. Crystallization kinetics in binary solid solution-aqueous solutions systems. *Am. J. Sci.* **2006**, *290*, 164–201. [[CrossRef](#)]